

Unitary Fermi gas at finite temperature in the expansion

Yusuke Nishida

Department of Physics, University of Tokyo, Tokyo 113-0033, Japan and
 Institute for Nuclear Theory, University of Washington, Seattle, Washington 98195-1550, USA
 (Dated: August 2006)

Thermodynamics of the unitary Fermi gas at finite temperature is investigated from the perspective of the expansion over $\beta = 4/d$ with d being the dimensionality of space. We show that the thermodynamics is dominated by bosonic excitations in the low temperature region $T < T_c$. Analytic formulas for the thermodynamic functions as functions of the temperature are derived to the lowest order in β in this region. In the high temperature region where $T > T_c$, bosonic and fermionic quasiparticles are excited. We determine the critical temperature T_c of the superfluid phase transition and the thermodynamic functions around T_c to the leading and next-to-leading orders in β .

PACS numbers: 03.75.Ss, 05.30.Fk, 05.70.Ce

I. INTRODUCTION

The Fermi gas with zero-range interaction at infinite scattering length [1,3], frequently referred to as the unitary Fermi gas, has attracted intense attention across many subfields of physics. Experimentally, the system can be realized in atomic traps using the Feshbach resonance and has been extensively studied [4-10]. Since the fermion density is the only dimensional scale of the unitary Fermi gas, its properties are universal, i.e., independent of details of the interparticle interaction. The unitary Fermi gas is an idealization of dilute nuclear matter and may be relevant to the physics of neutron stars [1]. It has been also suggested that its understanding may be important for the high- T_c superconductivity [12].

The austere simplicity of the unitary Fermi gas implies great difficulties for theoretical treatments, because there seems to be no parameter for a perturbation theory. Recently, we have proposed a new approach for the unitary Fermi gas based on the systematic expansion in terms of the dimensionality of space [13, 14], utilizing the speciality of four or two spatial dimensions in the unitarity limit [15]. In this approach, one would extend the problem to arbitrary spatial dimensions d and consider d is close to four or two. Then one performs all calculations treating $\beta = 4/d$ or $\beta = d/2$ as a small parameter for the perturbative expansion. Results for the physical case of three spatial dimensions are obtained by extrapolating the series expansions to $\beta = 1$, or more appropriately, by matching the two series expansions.

We used this expansion around four spatial dimensions to calculate thermodynamic functions and fermion quasiparticle spectrum in the unitarity limit and found results which are quite consistent with those obtained by Monte Carlo simulations and experiments [13, 14]. This expansion has been successfully applied to atom-dimer and dimer-dimer scatterings in vacuum [16]. Thus there

are compelling reasons to hope that the limit $d \rightarrow 4$ is not only theoretically interesting but also practically useful, despite the fact that the expansion parameter β is one at $d = 3$. Very recently, the phase structure of polarized Fermi gas near the unitarity point has been investigated based on the expansion [14, 17].

In this paper, we extend our approach to investigate the thermodynamics of unitary Fermi gas at finite temperature T , below and above the critical temperature $T = T_c$ of the superfluid phase transition. So far, such a problem has been studied relying on the mean-field description with fluctuations [18-28], the virial expansion [29-31], or the Monte Carlo simulations [32-36]. The main advantage of our approach is that $\beta = 4/d$ provides the small parameter of the perturbative expansion, and thus, analytic and systematic study below and above T_c is possible. We also note that the critical dimension of a superfluid-normal phase transition is also four, which makes weak-coupling calculations reliable at any temperature for the small β .

First, we review the expansion for the unitary Fermi gas around four spatial dimensions in Sec. II. Then we discuss that the thermodynamics in the low temperature region $T < T_c$ is dominated by bosonic excitations. Analytic formulas for the thermodynamic functions as functions of the temperature to the lowest order in β are shown in Sec. III. The behavior of the thermodynamic functions above T_c to the leading and next-to-leading orders in β is discussed in Sec. IV. In particular, we put emphasis on the determination of the critical temperature T_c by matching the expansion with the expansion around two spatial dimensions. The thermodynamic functions at T_c are also calculated, which are compared to the results from recent Monte Carlo simulations. Finally, summary and concluding remarks are given in Sec. V.

II. REVIEW OF EXPANSION

Here we briefly review the expansion for the unitary Fermi gas around four spatial dimensions and quote some results at zero temperature to the leading order in ϵ just for the convenience of later discussions at finite temperature. The detailed account of the expansion is found in Refs. [13, 14].

A. Lagrangian and Feynman rules

The extension to finite temperature T follows from the prescription of the imaginary time formalism. The system under consideration is described by the sum of following Lagrangian densities (here and below $\hbar = 1$ and $k_B = 1$):

$$L_0 = \psi^\dagger \left[\frac{3r^2}{2m} + \psi^\dagger \psi \right] + \psi^\dagger \left[\frac{r^2}{4m} \psi^\dagger + \frac{\psi^2}{c_0} \right]; \quad (1)$$

$$L_1 = g \psi^\dagger \psi + \psi^\dagger g \psi^\dagger \psi + \psi^\dagger \psi^3 + 2 \frac{g^2}{c_0} \psi^\dagger \psi + \frac{g_0}{c_0} \psi^\dagger + \frac{g_0}{c_0} \psi; \quad (2)$$

$$L_2 = \psi^\dagger \left[\frac{r^2}{4m} \psi^\dagger + 2 \psi^\dagger \psi \right]; \quad (3)$$

The propagators of fermion and boson are generated by L_0 . The fermion propagator G is a 2×2 matrix,

$$G(i\omega_n; p) = \frac{1}{(i\omega_n)^2 - E_p^2} \begin{pmatrix} i\omega_n + \mu_p & 0 \\ 0 & i\omega_n - \mu_p \end{pmatrix}; \quad (4)$$

where $\mu_p = p^2/2m$ is the kinetic energy of nonrelativistic particles and μ_0 chosen to be real is the condensate in the superfluid ground state. $E_p = \sqrt{\mu_p^2 + \frac{c_0^2}{4}}$ is the excitation energy of the fermion quasiparticle. The boson propagator D is given by

$$D(i\omega_n; p) = i\omega_n \frac{\mu_p}{2}; \quad (5)$$

$\omega_n = 2T(n + \frac{1}{2})$ and $\omega_n = 2Tn$ are discrete Matsubara frequencies for fermion and boson with an integer $n = 0; 1; 2; \dots$.

The unitary Fermi gas around four spatial dimensions is described by the weakly interacting system of fermionic and bosonic quasiparticles, whose coupling $g \sim \epsilon^{1/2}$ in L_1 is given by

$$g = \frac{(8\pi^2)^{1/2}}{m} \frac{m_0}{2} \epsilon^{-4}; \quad (6)$$

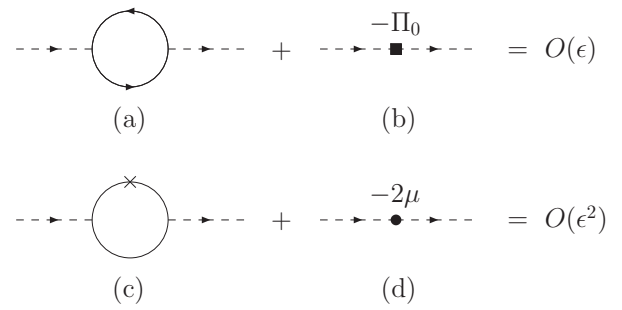


FIG. 1: Restoration of naive counting for the boson self-energy. The fermion loop in (c) goes around clockwise and counterclockwise. Solid (dotted) lines represent the fermion (boson) propagator G (D), while the cross in (c) represents the insertion to the fermion propagator.

The chemical potential μ_0 in L_1 is treated as a small perturbation in our formulation. We define the boson chemical potential as

$$\mu_b = 2 \frac{g^2}{c_0}; \quad (7)$$

In the dimensional regularization we use, when c_0 is negative, $g^2 = c_0 \mu_b$ gives the binding energy of the boson to the leading order in ϵ . Throughout this paper, we consider the vicinity of the unitary point where $\mu_b = 0$.

Finally the two additional vertices for the boson propagator in L_2 play a role of counter terms so as to avoid double counting of certain types of diagrams which are already taken into L_0 and L_1 . The first vertex in the momentum space is given by

$$V_0(p_0; p) = p_0 \frac{\mu_p}{2}; \quad (8)$$

B. Power counting rule of

The power counting rule of ϵ is summarized as follows.

1. We consider $\epsilon = 0$ and regard μ_0 as $O(1)$.
2. For any Green's function, we write down all Feynman diagrams according to the Feynman rules using the propagators from L_0 and the vertices from L_1 .
3. If there is any subdiagram of the type in Fig. 1 (a) or Fig. 1 (c), we add the same Feynman diagram where the subdiagram is replaced by a vertex from L_2 , Fig. 1 (b) or Fig. 1 (d).
4. The power of ϵ for the given Feynman diagram will be $O(\epsilon^{N_g = 2 + N})$, where N_g is the number of couplings g and N is the number of chemical potential insertions.

5. The only exception is the one-loop vacuum diagram of fermion with one insertion, which is $O(1)$ instead of the naive $O(d)$.

This power counting rule holds in the low temperature region where the condensate is still large compared to the chemical potential μ_0 , while it breaks down near the critical temperature because $\mu_0 \rightarrow 0$ at $T \rightarrow T_c$. In the high temperature region $T > T_c$, a modification of the power counting rule is necessary as we discuss at the beginning of Sec. IV.

C. Leading order results at $T = 0$

Here we show only lowest order results on the thermodynamic functions at zero temperature, which is equivalent to the mean-field approximation. The results up to the next-to-leading order in μ_0 are found in Refs. [13, 14]. The effective potential to the leading order in μ_0 is

$$V_e(\mu_0) = \frac{\mu_0^3}{3} - \frac{B}{2} \mu_0 + \frac{m^2 \mu_0^d}{2}; \quad (9)$$

from which the condensate follows as

$$\mu_0 = \frac{B}{2}; \quad (10)$$

Note that the previously made assumption $\mu_0 = O(d)$ is now checked. Then the pressure at zero temperature is given by

$$P_0 = V_e(\mu_0) = \frac{\mu_0^3}{6} - \frac{m^2 \mu_0^d}{2}; \quad (11)$$

From the fermion number density

$$N = \frac{\partial P_0}{\partial \mu_0} = \frac{1}{2} \mu_0^{d-1}; \quad (12)$$

we define the Fermi energy through the relationship in the ideal Fermi gas in d spatial dimensions;

$$\mu_F = \frac{2}{m} \left(\frac{1}{2} \mu_0^{d-1} + 1 \right)^{2/d} N^{2/d} = \frac{\mu_0^2}{2}; \quad (13)$$

Then the energy density is given by

$$E_0 = N \mu_F - P_0 = \frac{\mu_0^3}{3} - \frac{\mu_0^2}{2} + \frac{m^2 \mu_0^d}{2}; \quad (14)$$

where $\mu_b = \mu_0^2 = c_0 > 0$ is the binding energy of the boson. The chemical potential at the fixed Fermi energy μ_F is obtained from Eqs. (10) and (13) as

$$\mu_0 = \frac{3}{2} \mu_F + \frac{\mu_b}{2}; \quad (15)$$

$$\mu_B = \text{---} \times \text{---}$$

$$-\Pi_{11} = \text{---} \circ \text{---} + \text{---} \blacksquare \text{---}$$

$$-\Pi_{12} = \text{---} \circ \text{---}$$

FIG. 2: Boson's self-energy diagrams contributing to the order $O(d)$. The vertex μ_0 from L_2 needs to be added to the second diagram. The last diagram gives the off-diagonal part of the self-energy. Other elements are given by $\Pi_{22}(p) = \Pi_{11}(p)$ and $\Pi_{21}(p) = \Pi_{12}(p)$.

III. THERMODYNAMICS BELOW T_c

Now we investigate the thermodynamics of the Fermi gas at finite temperature near the unitarity limit. At zero temperature, we found that there exist two difference energy scales in the system; the scale of the condensate μ_0 and that of the chemical potential μ_0 . Accordingly, we can consider two temperature regions where the unitary Fermi gas exhibits different thermodynamics.

One is the low temperature region where $T < \mu_0$. In this region, the energy gap of the fermion quasiparticle excitation μ_0 is still large compared to the temperature. Therefore, thermal excitations of the fermion quasiparticle are exponentially suppressed by a factor $e^{-T/\mu_0} = e^{-1}$. The thermodynamics in this region is dominated by the bosonic phonon excitations. The other temperature region is the high temperature region where $T > \mu_0$. (μ_0 represents the condensate at zero temperature.) In this region, the condensate decreases and eventually vanishes at the critical temperature T_c . Fermions and bosons are equally excited here. We defer our discussion on the high temperature region to Sec. IV and concentrate on the thermodynamics in the low temperature region $T < T_c$ in this section.

A. Phonon spectrum

The thermodynamics in the low temperature region $T < \mu_0$ is dominated by the phonon excitations. In order to determine the phonon spectrum, we first study the boson self-energy at zero temperature. To the order of $O(d)$, there are three types of contributions to the boson self-energy as depicted in Fig. 2. In addition to the chemical potential insertion $\mu_B = 2 + \mu_b$, the one-loop diagrams contribute to the diagonal part $\Pi_{11}(p)$ and off-diagonal part $\Pi_{12}(p)$ of the boson self-energy. The vertex $\mu_0(p)$ from L_2 is necessary for $\Pi_{11}(p)$ according to the power counting rule described in Sec. II. Other elements can be

obtained from $\Sigma_{22}(\mathbf{p}) = \Sigma_{11}(\mathbf{p})$ and $\Sigma_{21}(\mathbf{p}) = \Sigma_{12}(\mathbf{p})$.

The diagonal part of the boson self-energy of $O(\mathbf{p})$ is given by the sum

$$\Sigma_{11}(\mathbf{p}) = \Sigma_0(\mathbf{p}) + \Sigma_a(\mathbf{p}); \quad (16)$$

$$\begin{aligned} \Sigma_a(\mathbf{p}) &= g^2 \int \frac{d\mathbf{k}_0 d\mathbf{k}}{(2\pi)^{d+1}} G_{11}\left(\mathbf{k} + \frac{\mathbf{p}}{2}\right) G_{22}\left(\mathbf{k} - \frac{\mathbf{p}}{2}\right) \\ &= g^2 \int_{\mathbf{k}} \frac{1}{4E_{\mathbf{k} - \frac{\mathbf{p}}{2}} E_{\mathbf{k} + \frac{\mathbf{p}}{2}}} \frac{(E_{\mathbf{k} - \frac{\mathbf{p}}{2}} + \epsilon_{\mathbf{k} - \frac{\mathbf{p}}{2}})(E_{\mathbf{k} + \frac{\mathbf{p}}{2}} + \epsilon_{\mathbf{k} + \frac{\mathbf{p}}{2}})}{E_{\mathbf{k} - \frac{\mathbf{p}}{2}} + E_{\mathbf{k} + \frac{\mathbf{p}}{2}} + \epsilon_0} + \frac{(E_{\mathbf{k} - \frac{\mathbf{p}}{2}} - \epsilon_{\mathbf{k} - \frac{\mathbf{p}}{2}})(E_{\mathbf{k} + \frac{\mathbf{p}}{2}} - \epsilon_{\mathbf{k} + \frac{\mathbf{p}}{2}})}{E_{\mathbf{k} - \frac{\mathbf{p}}{2}} + E_{\mathbf{k} + \frac{\mathbf{p}}{2}} + \epsilon_0} \end{aligned} \quad (17)$$

Here we introduced the shorthand notation,

$$\int_{\mathbf{k}} \frac{d\mathbf{k}}{(2\pi)^d} \quad (18)$$

Since we are interested in physics at the scale of temperature $T \ll T_0$, it is sufficient to evaluate the self-energy when the external momentum is small compared to the condensate $(\mathbf{p}_0; \epsilon_p) \ll T_0$. Expanding $\Sigma_{11}(\mathbf{p})$ in terms of $p=0$ and performing the \mathbf{k} integration with the use of the formula

$$\int_0^{\infty} dz \frac{z^1}{(z+1)^2} = \frac{1}{2} \quad (19)$$

we obtain

$$\Sigma_{11}(0) = g^2 \int_{\mathbf{k}} \frac{E_{\mathbf{k}}^2 + \epsilon_{\mathbf{k}}^2}{4E_{\mathbf{k}}^3} = \frac{3}{2} \epsilon_0 + O(\epsilon^2) \quad (20)$$

Similarly, the off-diagonal part of the boson self-energy of $O(\mathbf{p})$ is given by

$$\begin{aligned} \Sigma_{12}(\mathbf{p}) &= g^2 \int \frac{d\mathbf{k}_0 d\mathbf{k}}{(2\pi)^{d+1}} G_{12}\left(\mathbf{k} + \frac{\mathbf{p}}{2}\right) G_{12}\left(\mathbf{k} - \frac{\mathbf{p}}{2}\right) \\ &= g^2 \int_{\mathbf{k}} \frac{\epsilon_0}{4E_{\mathbf{k} - \frac{\mathbf{p}}{2}} E_{\mathbf{k} + \frac{\mathbf{p}}{2}}} \\ &= \frac{1}{E_{\mathbf{k} - \frac{\mathbf{p}}{2}} + E_{\mathbf{k} + \frac{\mathbf{p}}{2}} + \epsilon_0} + \frac{1}{E_{\mathbf{k} - \frac{\mathbf{p}}{2}} + E_{\mathbf{k} + \frac{\mathbf{p}}{2}} + \epsilon_0} \end{aligned} \quad (21)$$

Expanding $\Sigma_{12}(\mathbf{p})$ in terms of $p=0$ and performing the integration over \mathbf{k} , we obtain

$$\Sigma_{12}(0) = g^2 \int_{\mathbf{k}} \frac{\epsilon_0}{4E_{\mathbf{k}}^3} = \frac{1}{2} \epsilon_0 + O(\epsilon^2) \quad (22)$$

As a result of the resummation of these self-energies, the resummed boson propagator D is expressed by the following 2×2 matrix:

$$D(\mathbf{p}_0; \mathbf{p}) = \begin{pmatrix} D_{11}(\mathbf{p}) & D_{12}(\mathbf{p}) \\ D_{21}(\mathbf{p}) & D_{22}(\mathbf{p}) \end{pmatrix} \quad (23)$$

where $\Sigma_0(\mathbf{p})$ is defined in Eq. (8) and $\Sigma_a(\mathbf{p})$ is given by

where $\Sigma_{22}(\mathbf{p}) = \Sigma_{11}(\mathbf{p})$ and $\Sigma_{21}(\mathbf{p}) = \Sigma_{12}(\mathbf{p})$. Using the self-energies calculated above, the dispersion relation of the boson $\omega_{\text{ph}}(\mathbf{p})$ can be obtained by solving the equation $\det[D^{-1}(\mathbf{p}; \omega)] = 0$ in terms of ω as

$$\omega_{\text{ph}}(\mathbf{p}) = \frac{\epsilon_p}{2} \sqrt{\epsilon_B + \epsilon_0} \quad (24)$$

Note that this expression is valid as long as $\epsilon_p \ll T_0$ because of the expansions made to evaluate the boson self-energies. Substituting the solution of the gap equation at zero temperature in Eq. (10), $\epsilon_B = \epsilon_0$, the phonon spectrum is determined to be

$$\omega_{\text{ph}}(\mathbf{p}) = \frac{\epsilon_p}{2} \sqrt{\epsilon_0} \quad (25)$$

For the small momentum $\epsilon_p \ll T_0$, the dispersion relation becomes linear in the momentum as $\omega_{\text{ph}} \propto c_s p$, remaining gapless in accordance with the Nambu-Goldstone theorem. The sound velocity of phonon c_s is given by

$$c_s = \frac{\epsilon_0}{4m} + O(\epsilon^{3=2}), \quad v_F = \frac{\epsilon_0}{8} \quad (26)$$

where $v_F = (2\epsilon_F = m)^{1=2}$ is the Fermi velocity. For the large momentum $\epsilon_p \gg T_0$, the dispersion relation approaches that of the free boson as $\omega_{\text{ph}} \propto \epsilon_p = 2$.

B. Effective potential and condensate

At finite temperature, the phonon excitations contribute to the effective potential, and consequently, the magnitude of the condensate decreases. The temperature dependent part of the effective potential $V_T(\epsilon_0)$ to the lowest order in ϵ is given by the one-loop diagram of the boson with the resummed propagator in Eq. (23)

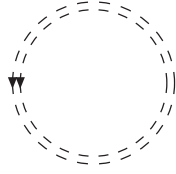


FIG. 3: One-loop diagram of boson contributing to the effective potential at finite temperature. The dotted double line represents the resummed boson propagator D in Eq. (23).

(Fig. 3):

$$V_T(\mu_0) = \frac{T}{2} \sum_{\mathbf{p}} \text{Tr} \ln D(i\omega_n; \mathbf{p})^{-1} \quad (27)$$

$$= T \sum_{\mathbf{p}} \ln 1 - e^{i\omega_n(\mathbf{p})=T} \quad (27)$$

The n -point interaction vertex among phonons Γ^n is of the order μ^{n-2} and appears in the effective potential only at higher orders. Then the contribution of $V_T(\mu_0)$ to the gap equation is

$$\frac{\partial V_T(\mu_0)}{\partial \mu_0} = \sum_{\mathbf{p}} f_B(i\omega_{\mathbf{p}}) \frac{\partial i\omega_{\mathbf{p}}}{\partial \mu_0}; \quad (28)$$

where $f_B(x) = 1/(e^{x/T} - 1)$ is the Bose distribution function and $\partial i\omega_{\mathbf{p}}/\partial \mu_0$ is given from Eq. (24) by

$$\frac{\partial i\omega_{\mathbf{p}}}{\partial \mu_0} = \frac{3\mu_{\mathbf{p}} + 2\mu_0}{4i\omega_{\mathbf{p}}}; \quad (29)$$

There are two limiting cases where the integration over \mathbf{p} in Eq. (28) can be analytically performed. Since the integral is dominated by the integration region where $\mu_{\mathbf{p}} \ll T$, we can approximate the phonon spectrum by its linear branch $i\omega_{\mathbf{p}}(\mathbf{p}) \approx c_s p$ when the temperature is very low $T \ll \mu_0$. In this case, the integration over \mathbf{p} at $d = 4$ leads to

$$\frac{\partial V_T(\mu_0)}{\partial \mu_0} \approx \frac{8}{3} \frac{(3)T}{\mu_0} \frac{mT}{2}; \quad (30)$$

On the other hand, when the temperature is located in the intermediate region $\mu_0 \ll T \ll \mu_0$, the phonon spectrum can be approximated by its quadratic branch $i\omega_{\mathbf{p}} \approx \mu_{\mathbf{p}}^2$. In this case, the integration over \mathbf{p} in Eq. (28) at $d = 4$ results in

$$\frac{\partial V_T(\mu_0)}{\partial \mu_0} \approx \frac{(mT)^2}{4}; \quad (31)$$

Now, from the gap equation $\partial[V_e(\mu_0) + V_T(\mu_0)]/\partial \mu_0 = 0$ with $\mu_0 = \mu_0 + T$, one finds the temperature dependent correction of the condensate T satisfies

$$\frac{\partial V_e(\mu_0)^2}{\partial \mu_0^2} T + \frac{\partial V_T(\mu_0)}{\partial \mu_0} = 0; \quad (32)$$

where $V_e(\mu_0)$ is the effective potential at zero temperature in Eq. (9). To the leading order in T/μ_0 , T at $T \ll \mu_0$ is given by

$$T = \frac{8}{3} \frac{(3)T^3}{\mu_0^2}; \quad (33)$$

while at $\mu_0 \ll T \ll \mu_0$,

$$T = \frac{2T^2}{\mu_0}; \quad (34)$$

The condensate in total is $\mu_0 = \mu_0 + T$, which decreases as the temperature increases. Note that since $T \ll \mu_0$, the leading part of the condensate does not change in the temperature region considered here $T \ll \mu_0$. The effective potential is given by the sum of the zero temperature and finite temperature parts; $V_e(\mu_0 + T) + V_T(\mu_0 + T) \approx V_e(\mu_0) + V_T(\mu_0)$.

C. Thermodynamic functions at low temperature

The temperature dependent part of the pressure P_{ph} in the low temperature region $T \ll \mu_0$ is given from the effective potential in Eq. (27) by

$$P_{\text{ph}} = -V_T(\mu_0) = T \sum_{\mathbf{p}} \ln 1 - e^{i\omega_{\mathbf{p}}(\mathbf{p})=T} \quad (35)$$

The phonon contributions to the fermion number density, the entropy density, and the energy density are respectively computed from the thermodynamic relations, $N_{\text{ph}} = \partial P_{\text{ph}}/\partial \mu$, $S_{\text{ph}} = \partial P_{\text{ph}}/\partial T$, and $E_{\text{ph}} = N_{\text{ph}} + TS_{\text{ph}} - P_{\text{ph}}$. Here we show analytic expressions for these thermodynamic functions in the two cases where the analytic evaluation of the \mathbf{p} integration in Eq. (35) is available.

When the temperature is very low $T \ll \mu_0$, only the linear branch of the phonon spectrum $i\omega_{\mathbf{p}}(\mathbf{p}) \approx c_s p$ is important to the thermodynamic functions. In this case, the integration over \mathbf{p} at $d = 4$ can be performed analytically to lead to

$$P_{\text{ph}} \approx \frac{12}{(2)^4} \frac{(5)T^5}{c_s^4} = \frac{12}{2} \frac{(5)m^2 T^5}{(\mu_0)^2}; \quad (36)$$

Note that the exponent of T in general spatial dimension d is $P_{\text{ph}} \propto T^{d+1}$. Accordingly, we obtain the phonon contributions to the fermion number density, the entropy density, and the energy density:

$$N_{\text{ph}} = \frac{48}{2} \frac{(5)m^2 T^5}{(\mu_0)^3}; \quad (37)$$

$$S_{\text{ph}} = \frac{60}{2} \frac{(5)m^2 T^4}{(\mu_0)^2}; \quad (38)$$

$$E_{\text{ph}} = \frac{24}{2} \frac{(5)m^2 T^5}{(\mu_0)^2} \left(1 + \frac{\mu_b}{\mu_0} \right); \quad (39)$$

Since actual experiments or simulations are performed with the fixed fermion density, it is useful to show the thermodynamic functions at fixed N instead of fixed μ . From Eqs. (10), (12), and (37), we find the chemical potential for the fixed fermion density increases as a function of the temperature as

$$\mu = \mu_0 + 48 \left(\frac{T}{\mu_0} \right)^5; \quad (40)$$

where μ_0 represents the chemical potential at zero temperature in Eq. (15). Normalizing by the Fermi energy in Eq. (13), we have

$$\frac{\mu}{\mu_F} = \frac{\mu_0}{\mu_F} + \frac{3}{2} \left(\frac{T}{\mu_F} \right)^5; \quad (41)$$

The other thermodynamic functions for the fixed fermion number density are given by

$$\frac{P}{\mu_F N} = \frac{P_0}{\mu_F N} + \frac{3}{3} \left(\frac{T}{\mu_F} \right)^5; \quad (42)$$

$$\frac{E}{\mu_F N} = \frac{E_0}{\mu_F N} + \frac{6}{3} \left(\frac{T}{\mu_F} \right)^5; \quad (43)$$

$$\frac{S}{N} = \frac{15}{3} \left(\frac{T}{\mu_F} \right)^4; \quad (44)$$

These expressions are valid in the low temperature region where $T \ll \mu_0$ and hence $T = \mu_F^{3=2}$. The exponent of T is different from that in three spatial dimensions because we are expanding around four spatial dimensions. The correct exponent at $d = 3$ is recovered if we resum logarithmic corrections $(\ln T^n)$ to infinite orders, which are formally higher orders in μ_0 and are not shown in the formulas above.

On the other hand, when the temperature is located in the intermediate region $\mu_0 \ll T \ll \mu_0$, we can expand the phonon spectrum $\epsilon_{ph}(\mathbf{p})$ in terms of $\mu_0 = \mu_p$ up to its first order

$$\epsilon_{ph}(\mathbf{p}) \approx \frac{\mu_p}{2} + \frac{0}{2}; \quad (45)$$

In this case, the integration over \mathbf{p} in Eq. (35) at $d = 4$ can be performed analytically again to result in

$$P_{ph} \approx \frac{(3)}{2} m^2 T^3 - \frac{m^2 T^2}{12} \mu_0; \quad (46)$$

Note that the exponent of T in general spatial dimension d is $P_{ph} \propto T^{d=2+1} + T^{d=2}$. Accordingly, we obtain the temperature dependent parts of the fermion number density, the entropy density, and the energy density:

$$N_{ph} = \frac{m^2 T^2}{6}; \quad (47)$$

$$S_{ph} = \frac{3}{2} \left(\frac{T}{\mu_0} \right) m^2 T^2 - \frac{m^2 T}{6} \mu_0; \quad (48)$$

$$E_{ph} = \frac{2}{2} \left(\frac{T}{\mu_0} \right) m^2 T^3 - \frac{m^2 T^2}{6} \mu_0 - \frac{\mu_b}{2} \mu_0; \quad (49)$$

From Eqs. (10), (12), and (47), we find the chemical potential for the fixed fermion density increases as a function of the temperature as

$$\mu = \mu_0 + \frac{2}{6} \frac{T^2}{\mu_0}; \quad (50)$$

Normalizing by the Fermi energy in Eq. (13), we have

$$\frac{\mu}{\mu_F} = \frac{\mu_0}{\mu_F} + \frac{3=2}{6} \frac{T}{\mu_F}^2; \quad (51)$$

The other thermodynamic functions for the fixed fermion number density are given by

$$\frac{P}{\mu_F N} = \frac{P_0}{\mu_F N} + 4 \left(\frac{T}{\mu_F} \right)^3 - \frac{3=2}{6} \frac{T}{\mu_F}^2; \quad (52)$$

$$\frac{E}{\mu_F N} = \frac{E_0}{\mu_F N} + 8 \left(\frac{T}{\mu_F} \right)^3 - \frac{3=2}{3} \frac{T}{\mu_F}^2; \quad (53)$$

$$\frac{S}{N} = 12 \left(\frac{T}{\mu_F} \right)^2 - \frac{3=2}{3} \frac{T}{\mu_F}; \quad (54)$$

These expressions are valid in the intermediate temperature region where $\mu_0 \ll T \ll \mu_0$ and hence $T = \mu_F^{3=2}$. The exponent of T is different from that in three spatial dimensions because we are expanding around four spatial dimensions. The correct exponent at $d = 3$ is recovered if we resum logarithmic corrections $\frac{1}{2} \ln T^n$ to infinite orders, which are formally higher orders in μ_0 and are not shown in the formulas above.

D. Effective potential near T_c

At the end of this section, we study the behavior of the condensate ϕ as a function of the temperature for a given μ . The effective potential to the leading order in μ is given by one-loop diagrams of fermion with and without one insertion, which is equivalent to the mean-field approximation. Since the critical dimension of the superfluid-normal phase transition is four, the mean-field approximation remains as a leading part at any temperature in the limit $d \rightarrow 4$. Then the leading contribution to the effective potential at finite temperature is given by

$$V_e(\phi) = \frac{\mu_b}{g^2} \int \frac{d^4 p}{(2\pi)^4} E_p \frac{\mu_p}{E_p} + 2T \ln \int \frac{d^4 p}{(2\pi)^4} 1 + e^{E_p = T}; \quad (55)$$

where $f_F(x) = 1/(e^{x-T} + 1)$ is the Fermi distribution function.

For the low temperature $T \ll \mu_0$, we can neglect the exponentially small factor $e^{E_p = T} \ll 1$ and the integration over \mathbf{p} reproduces the effective potential at zero temperature in Eq. (9). In the opposite limit where $T \gg \mu_0$, we can expand $V_e(\phi)$ in terms of $\mu_0 = T$ to lead to

$$V_e(\phi) \approx V_e(0) + \frac{h}{T} \ln 2 - \frac{B}{2} \frac{i}{2} \frac{m}{2}^2 + \frac{2}{16T} \frac{m}{2}^2 + \dots; \quad (56)$$

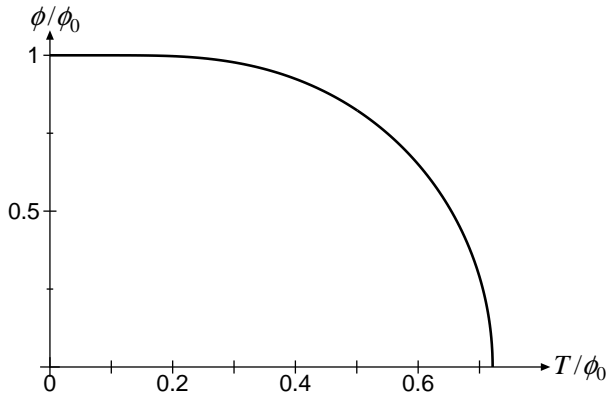


FIG. 4: The behavior of the condensate ϕ as a function of the temperature T to the lowest order in ϵ . $\phi_0 = \phi_B = 1$ is the value of the condensate at $T = 0$ and the critical temperature is located at $T_c = \phi_0 = 1 = (2 \ln 2)^{-1} \approx 0.721348$.

where $\phi_B = 2 + \epsilon_b$. From the coefficient of the quadratic term in ϵ , we can read the critical temperature T_c of the second order phase transition to the leading order in ϵ as

$$T_c = \frac{\phi_B}{2 \ln 2} + O(\epsilon); \quad (57)$$

and the value of the condensate just below T_c as

$$\phi^2 = 8T_c (T_c - T) \ln 2 + O(\epsilon); \quad (58)$$

The condensate in the intermediate range of the temperature is obtained by solving the gap equation $\partial V_e / \partial \phi = 0$:

$$-\frac{\phi_B}{2} + \sum_p \frac{2\epsilon_p}{E_p} f_F(E_p) = 0; \quad (59)$$

The numerical solution of the gap equation as a function of T is shown in Fig. 4.

Finally we note that critical exponents for an $O(2)$ -symmetric theory will be in principle recovered if we resum logarithmic corrections $(\epsilon \ln |T - T_c|)^n$ appearing at higher orders due to the infrared physics of bosons with a zero Matsubara frequency. [We can see such a logarithmic correction, e.g., in Eq. (69).] Resumming these logarithmic corrections to infinite orders, the critical exponent shifts from its mean-field value by $|T - T_c|^{-\epsilon}$ to produce the known results for the XY universality class in the usual expansion. In other words, we cannot see the shift of the critical exponent at finite orders in our expansion.

C. Pressure

Now we calculate the thermodynamic functions at $T = T_c$ to the leading and next-to-leading orders in ϵ . There are three types of diagrams contributing to the pressure up to the next-to-leading order in ϵ as depicted in Fig. 5; one-loop diagrams of fermion (boson) with and without one (ϕ_B) insertion and two-loop diagram with a boson exchange. Note that at $T = T_c$, the boson's one-loop diagram contributes as $O(1)$ as well as the fermion's one-loop

IV. THERMODYNAMICS ABOVE T_c

A. Power counting rule of ϕ near T_c

In the expansion at zero or low temperature, the chemical potential is small compared to the condensate ϕ_0 and we made expansions in terms of $\epsilon = \phi_0^{-1}$ as well as the small coupling $g^{-1=2}$. Near the critical temperature, the ratio $\epsilon = \phi_0^{-1}$ is no longer small because the condensate vanishes at $T = T_c$, while $\epsilon = T_c^{-1}$ is $O(\epsilon)$ as it is clear from $T_c = \phi_B = (2 \ln 2)^{-1}$ in Eq. (57). Therefore, we can still treat the chemical potential as a small perturbation near T_c and the same power counting rule of ϕ described in Sec. II B holds even above T_c just by replacing ϕ_0 with T . Hereafter we regard $T = T_c$ as $O(1)$.

B. Boson's thermal mass

First we study the self-energy of boson at $T = T_c$. The leading contribution to the self-energy is the chemical potential insertion ϕ_B as well as the one-loop diagram Π_1 shown in Fig. 2:

$$\begin{aligned} \Pi_1(i; p) &= \sum_k \frac{1}{Z} \Pi_1^0(i; p) \\ &= g^2 T \sum_k G_{11}(i; n + i; k + p) G_{22}(i; n; k) \\ &= g^2 \sum_k \frac{1}{2\epsilon_k} \frac{f_F(\epsilon_{k+p=2})}{i + \epsilon_{p=2}}: \quad (60) \end{aligned}$$

For the zero Matsubara frequency mode $\epsilon_n = 0$ at the small momentum $\epsilon_p = T$, we have

$$\Pi_1(0; 0) = g^2 \sum_k \frac{f_F(\epsilon_k)}{\epsilon_k} = T 2 \ln 2 + O(\epsilon^2); \quad (61)$$

Therefore, the zero Matsubara frequency mode has the non-negative thermal mass $\epsilon_T = T 2 \ln 2 - \phi_B = O(\epsilon)$ at $T = T_c$. The condition of the vanishing thermal mass $\epsilon_T = 0$ gives the critical temperature $T_c = \phi_B = (2 \ln 2)^{-1} + O(\epsilon)$ equivalent to Eq. (57). As we will see below, at a sufficiently high order in the perturbation theory near T_c [$O(\epsilon^2)$ or $O(\epsilon)$ compared to the leading term in the pressure or fermion density], a resummation of the boson self-energy is needed to avoid infrared singularities appearing in the zero Matsubara frequency mode.

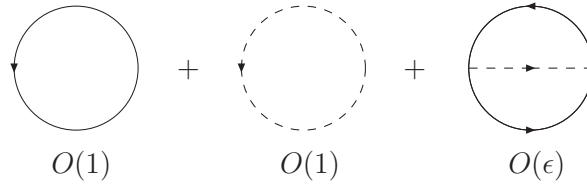


FIG. 5: Three types of diagrams contributing to the pressure up to the next-to-leading order in ϵ . Each (B) insertion to the fermion (boson) line reduces the power of ϵ by one.

diagram. Then the pressure from the one-loop diagrams is given by

$$\begin{aligned}
 P_1 &= \int_p \frac{d^d p}{(2\pi)^d} \ln \left[1 + e^{-\beta \epsilon_p} \right] + 2 \int_p \frac{d^d p}{(2\pi)^d} \ln \left[1 + e^{-\beta \epsilon_p} \right] + 2 \int_p \frac{d^d p}{(2\pi)^d} f_F(\epsilon_p) + \int_p \frac{d^d p}{(2\pi)^d} f_B(\epsilon_p) \\
 &= T \frac{11}{2} \zeta(3) - \frac{9 \ln 2}{4} \zeta(3) + \frac{11}{4} \zeta(3) + \frac{2}{6} \frac{m^2}{T} + \frac{2}{3} \frac{m_B^2}{T} - \frac{m T}{2} \zeta(d=2)
 \end{aligned} \quad (62)$$

The contribution from the two-loop diagram to the pressure, which is $O(\epsilon^2)$, is given by

$$\begin{aligned}
 P_2 &= g^2 T^2 \int_{p,q} \frac{d^d p}{(2\pi)^d} \frac{d^d q}{(2\pi)^d} G_{11}(i_n; p) G_{22}(i_m; q) D(i_n, i_m; p, q) \\
 &= g^2 \int_{p,q} \frac{d^d p}{(2\pi)^d} \frac{d^d q}{(2\pi)^d} \frac{f_F(\epsilon_p) f_F(\epsilon_q) + [f_F(\epsilon_p) + f_F(\epsilon_q)] f_B(\epsilon_{p+q})}{\epsilon_p + \epsilon_q - \epsilon_{p+q}}
 \end{aligned} \quad (63)$$

The numerical integrations over p and q result in

$$P_2 = C_p \frac{m T}{2} \zeta(d=2)
 \quad (64)$$

where $C_p = 8.4144$ is a numerical constant. From Eqs. (62) and (64), we obtain the pressure up to the next-to-leading order in ϵ as

$$P = P_1 + P_2 = T \frac{11}{2} \zeta(3) - \frac{9 \ln 2}{4} \zeta(3) + \frac{11}{4} \zeta(3) + \frac{2}{6} \frac{m^2}{T} + \frac{2}{3} \frac{m_B^2}{T} - \frac{m T}{2} \zeta(d=2) + C_p \frac{m T}{2} \zeta(d=2)
 \quad (65)$$

The entropy density S and the energy density E to the same order can be computed from the thermodynamic relations $S = \partial P / \partial T$ and $E = N + T S - P$.

D. Fermion number density

The fermion number density to the next-to-leading order in ϵ cannot be obtained simply by differentiating the pressure in Eq. (65) with respect to the chemical potential $N = \partial P / \partial \mu$. Since the pressure to the leading order in ϵ does not depend on μ and the derivative $\partial / \partial \mu = \partial / \partial \epsilon$ enhances the power of ϵ by one, we need to compute the one-loop diagrams with two (B) insertions and the two-loop diagrams with one (B) insertion. The fermion density from the fermion's one-loop diagrams is given by

$$\begin{aligned}
 N_F &= 2 \int_p \frac{d^d p}{(2\pi)^d} f_F(\epsilon_p) + \frac{1}{T} \int_p \frac{d^d p}{(2\pi)^d} f_F(\epsilon_p) f_F(\epsilon_p) \\
 &= \frac{2}{6} \zeta(2) - \frac{2 \ln 2}{12} \zeta(2) + \frac{2 \ln 2}{T} - \frac{m T}{2} \zeta(d=2)
 \end{aligned} \quad (66)$$

On the other hand, the boson's one-loop diagrams contribute to the fermion density as

$$N_B = 2 \int_p \frac{d^d p}{(2\pi)^d} f_B(\epsilon_p) - \frac{1}{T} \int_p \frac{d^d p}{(2\pi)^d} f_B(\epsilon_p) f_B(\epsilon_p)
 \quad (67)$$

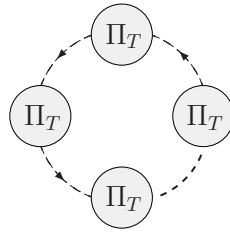


FIG. 6: A type of diagrams resummed to resolve the infrared singularity in Eq. (67).

Apparently, the last term has an infrared singularity because the Bose distribution function behaves as $f_B(\mu_p=2) \sim 2T=\mu_p$ at small momentum $\mu_p \rightarrow T$. In order to resolve this infrared singularity, the resummation of the boson self-energy $\Pi_T = \Pi_{11}^B(\mu_p=0)$ is needed at the small momentum region $\mu_p \rightarrow T$. After resumming a type of diagrams shown in Fig. 6, we can rewrite N_B within the accuracy we are working as

$$N_B = 2 \int_p [f_B(\mu_p=2 + \Pi_T) - 2 \ln 2 f_B(\mu_p=2) f_B(\mu_p=2)] + O(\epsilon^2); \quad (68)$$

where we used $\Pi_{11}^B = T = 2 \ln 2$. Now the first term is infrared finite, where the boson's thermal mass Π_T plays a role of an infrared cutoff. Integrating over p and expanding up to the next-to-leading order in ϵ , we have

$$2 \int_p f_B(\mu_p=2 + \Pi_T) = \frac{4}{3} \int_p \frac{2 \ln 2 + 12 \ln^0(2)}{3} - 8 \ln \frac{T}{T} + \frac{T}{T} + O(\epsilon^2) = \frac{m T}{2} \quad (69)$$

The logarithmic term $\ln T = T$ appears as a consequence of the resummation. The second term in Eq. (68), which is still infrared divergent, will cancel with the infrared singularity existing in the two-loop diagram.

The contribution from the two-loop diagrams to the fermion density is given by

$$N_2 = \int_{pk}^Z \frac{f_F(\mu_{k+p=2}) f_F(\mu_{k+p=2}) f_F(\mu_{k=p=2}) + f_B(\mu_p=2) - 2 f_F(\mu_{k+p=2}) f_B(\mu_p=2) f_B(\mu_p=2)}{\mu_k T}; \quad (70)$$

The second term in the numerator contains the infrared singularity at small μ_p . Extracting the divergent part, we can rewrite N_2 as

$$N_2 = \int_{pk}^Z \frac{f_F(\mu_{k+p=2}) f_F(\mu_{k+p=2}) f_F(\mu_{k=p=2}) + f_B(\mu_p=2) - 2 f_F(\mu_{k+p=2}) f_B(\mu_p=2) f_B(\mu_p=2)}{\mu_k T} + 2g^2 \int_{pk}^Z \frac{f_F(\mu_k)}{\mu_k T} f_B(\mu_p=2) f_B(\mu_p=2); \quad (71)$$

Now the first term is infrared finite. One finds the k integration in the second term can be performed to lead to $\Pi_{11} = T 2 \ln 2$ in Eq. (61), which exactly cancels out the infrared divergent part in Eq. (68). The numerical integrations over k and p in the first term result in

$$N_2 = C_N \frac{m T}{2} + 4 \ln 2 \int_p f_B(\mu_p=2) f_B(\mu_p=2); \quad (72)$$

where $C_N = 1.92181$ is a numerical constant.

Gathering up all contributions, Eqs. (66), (68), and (72), the fermion number density to the leading and next-to-leading orders in ϵ is given by

$$N = N_F + N_B + N_2 = \frac{3}{2} \int_p \frac{3 \ln 2 + 18 \ln^0(2)}{4} + \frac{2 \ln 2}{T} - 8 \ln \frac{T}{T} + \frac{T}{T} = \frac{m T}{2} \quad (73)$$

We define the Fermi energy μ_F through the relationship in Eq. (13) as

$$\frac{\mu_F}{T} = \frac{3}{2} \int_p \frac{3 \ln 2 + 18 \ln^0(2)}{4} + \frac{C_N}{3} + \frac{1}{8} \ln \frac{3}{2} + \frac{2 \ln 2}{3 \ln^2 T} - \frac{8}{3 \ln^2 T} \ln \frac{T}{T} = \frac{m T}{2} \quad (74)$$

The logarithmic correction $(T=T) \ln T = T \ln$ is a consequence of the resummation in the infrared physics of bosons with the zero Matsubara frequency, while it vanishes just at the critical temperature $T_c = T_c 2 \ln 2 = 0$.

E. Critical temperature

The critical temperature in units of the Fermi energy directly follows from Eq. (74) with the use of the rela-

tionship $2 + \mu_b = T_c 2 \ln 2$:

$$\begin{aligned} \frac{T_c}{\mu_F} &= \frac{r}{3^2} \left(1 + \frac{2}{8} \frac{3}{2 \ln 2} + \frac{3^0(2)}{2^2} \frac{C_N}{3^2} + \frac{1}{8} \ln \frac{3}{2} + \frac{\ln 2}{3^2} \frac{\mu_b}{\mu_F} \right) \\ &= 0.260 + 0.0112 + 0.0234 \frac{\mu_b}{\mu_F} + O(\epsilon^2); \end{aligned} \quad (75)$$

where the numerical value $C_N = 1.92181$ is substituted. We find the critical temperature T_c is an increasing function of the binding energy μ_b near the unitarity limit. The next-to-leading-order correction is reasonably small compared to the leading term even at $\epsilon = 1$. The naive extrapolation of the critical temperature to the physical case of $d = 3$ gives $T_c = \mu_F = 0.249$ in the unitarity limit $\mu_b = 0$. This value is surprisingly close to results from two Monte Carlo simulations, $T_c = \mu_F = 0.23(2)$ [33] and $T_c = \mu_F = 0.25$ [36], while other two simulations provide smaller values, $T_c = \mu_F < 0.14$ [34] and $T_c = \mu_F = 0.152(7)$ [35].

It is also interesting to compare the critical temperature in the unitarity limit with that in the BEC limit T_{BEC} . In the BEC limit, all fermion pairs are con ned into tightly bound molecules and the system becomes a noninteracting Bose gas where the boson mass is $2m$ and the boson density is $N=2$. The critical temperature for the Bose-Einstein condensation of such an ideal Bose gas at $d > 2$ spatial dimensions becomes

$$\frac{T_{BEC}}{\mu_F} = \frac{1}{2} \left(\frac{d}{2} \right)^{2-d} \left(1 + \frac{d}{2} \right)^{-2/d}; \quad (76)$$

To the leading and next-to-leading orders in $\epsilon = 4 - d$, the ratio of the critical temperatures in the unitarity limit T_c and in the BEC limit T_{BEC} at the same fermion density is given by

$$\begin{aligned} \frac{T_c}{T_{BEC}} &= \frac{r}{8} \left(1 + 0.0177 \epsilon + O(\epsilon^2) \right) \\ &= 0.943 + 0.0167 \epsilon + O(\epsilon^2); \end{aligned} \quad (77)$$

The ratio is slightly below unity, indicating the lower critical temperature in the unitarity limit $T_c < T_{BEC}$. The leading order term of the above ratio, $T_c = T_{BEC} = \sqrt{8=9}$, has the following clear physical interpretation: The critical temperature for the Bose-Einstein condensation at $d = 4$ is proportional to a square root of the boson's density. In the BEC limit, all fermion pairs form the bound bosons, while only 8 of 9 fermion pairs form the bosons and 1 of 9 fermion pairs is dissociated in the unitarity

limit [see the leading order terms of fermion and boson densities in Eqs. (66) and (69)]. Thus their ratio in the critical temperature should be $T_c = T_{BEC} = \sqrt{8=9} < 1$ at $d = 4$.

The more appropriate estimate of T_c at $d = 3$ will be obtained by matching the expansion around four spatial dimensions with the exact result around $d = 2$. The critical temperature at unitarity in the expansion over $\epsilon = d - 2$ is given by $T_c = (e = \epsilon)$, where $\epsilon = \mu_F = (2=e) e^{1=}$ is the energy gap of the fermion quasiparticle at zero temperature [14]:

$$\frac{T_c}{\mu_F} = \frac{2e^{-1}}{e^{1=}} \left(1 + O(\epsilon) \right); \quad (78)$$

We shall write the power series of T_c in the form of the Borel transformation,

$$\frac{T_c(\epsilon)}{\mu_F} = \frac{2e^{-1}}{e^{1=}} e^{1= \int_0^Z dt e^{-t} B_{T_c}(t)}; \quad (79)$$

$B_{T_c}(t)$ is the Borel transform of the power series in $T_c(\epsilon)$, whose Taylor coefficients at origin is given by $B_{T_c}(t) = 1 + \dots$. In order to perform the integration over t in Eq. (79), the analytic continuation of the Borel transform $B_{T_c}(t)$ to the real positive axis of t is necessary. Here we employ the Padé approximant, where $B_{T_c}(t)$ is replaced by the following rational functions

$$B_{T_c}(t) = \frac{1 + p_1 t + \dots + p_M t^M}{1 + q_1 t + \dots + q_N t^N}; \quad (80)$$

Then we incorporate the results around four spatial dimensions in Eq. (75) by imposing

$$\frac{T_c(2 - \epsilon)}{\mu_F} = 0.260 + 0.0112 \epsilon + \dots \quad (81)$$

on the Padé approximants as a boundary condition. Since we have two known coefficients from the expansion, the Padé approximants $[M/N]$ satisfying $M + N = 2$ are possible. Since we could not find a solution satisfying the boundary condition in Eq. (81) for $[M/N] = [1=1]$, we adopt other two Padé approximants with $[M/N] =$

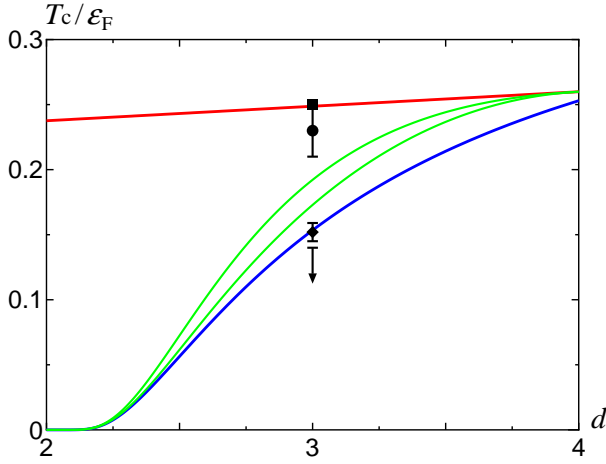


FIG. 7: (Color online) The critical temperature T_c at unitarity as a function of the spatial dimension d . The upper solid line is from the expansion around $d = 4$ in Eq. (75), while the lower solid curve is from the expansion around $d = 2$ in Eq. (78). The middle two curves show the different Borel-Pade approximations connecting the two expansions. The symbols at $d = 3$ indicate the results from the Monte Carlo simulations; $T_c/\epsilon_F = 0.23(2)$ [33] (circle), $T_c/\epsilon_F < 0.14$ [34] (down arrow), $T_c/\epsilon_F = 0.152(7)$ [35] (diamond), and $T_c/\epsilon_F = 0.25$ [36] (square).

$[2=0]$; $[0=2]$, whose coefficients p_m and q_n are determined uniquely by the above conditions.

Figure 7 shows the critical temperature T_c in units of the Fermi energy ϵ_F as a function of the spatial dimension d . The middle two curves show T_c/ϵ_F in the different Pade approximations connecting the two expansions around $d = 4$ and $d = 2$. These Borel-Pade approximations give $T_c/\epsilon_F = 0.173$ and 0.192 at $d = 3$, which are located between the naive extrapolations to $d = 3$ from the $d = 4$ expansion ($T_c/\epsilon_F = 0.249$) and the $d = 2$ expansion ($T_c/\epsilon_F = 0.153$). It is also interesting to compare our results with those from the recent Monte Carlo simulations, where $T_c/\epsilon_F = 0.23(2)$ [33], $T_c/\epsilon_F < 0.14$ [34], $T_c/\epsilon_F = 0.152(7)$ [35], and $T_c/\epsilon_F = 0.25$ [36]. Although these results from the Monte Carlo simulations seem not to be settled, the interpolation of the two expansions provides the moderate value $T_c/\epsilon_F = 0.183 \pm 0.014$ not too far from the Monte Carlo simulations.

F. Thermodynamic functions at T_c

Finally we show the thermodynamic functions at T_c in the unitarity limit $b = 0$ to the leading and next-to-leading orders in ϵ . The pressure P normalized by the fermion density n_F follows from Eqs. (65), (73), and (74). Introducing the numerical values $C_P = 8.4144$ and $C_N = 1.92181$, we obtain the pressure up to the next-to-

leading order in ϵ as

$$\frac{P}{n_F n_{T_c}} = 0.116 + 0.0188 \epsilon : \quad (82)$$

From the universal relationship in the unitarity limit $E = (d-2)P$, the energy density is given by

$$\frac{E}{n_F n_{T_c}} = 0.232 - 0.0205 \epsilon : \quad (83)$$

The chemical potential at the critical temperature $\mu = T_c \ln 2$ is $O(\epsilon)$. Normalizing by the Fermi energy in Eq. (75), we have

$$\frac{\mu}{\epsilon_F} = \ln 2 \frac{2}{3^{1/2}} = 0.180 : \quad (84)$$

Then the entropy density $T_c S = (d-2+1)P/n_F$ is given by

$$\frac{S}{N_{T_c}} = 1.340 - 0.642 \epsilon : \quad (85)$$

The next-to-leading-order corrections in the pressure and energy density are reasonably small compared to the leading order terms, while that is large for the entropy density.

We match the thermodynamic functions at T_c in the expansions over $d = 4 - d$ with those around $d = 2$ as we demonstrated for T_c/ϵ_F . The critical temperature around $d = 2$ is $T_c/\epsilon_F = e^{1-\epsilon}$, which is exponentially small and negligible compared to any power series of ϵ . Therefore, the pressure, the energy density, and the chemical potential at T_c in the expansions over $d = 2$ are simply given by those at zero temperature [14]:

$$\frac{P}{n_F n_{T_c}} = \frac{2}{d+2} = \frac{1}{2} - \frac{5}{8} \epsilon ; \quad (86)$$

$$\frac{E}{n_F n_{T_c}} = \frac{d}{d+2} = \frac{1}{2} - \frac{3}{8} \epsilon ; \quad (87)$$

$$\frac{\mu}{\epsilon_F} = 1 - \epsilon : \quad (88)$$

A straightforward calculation shows that the entropy per particle at T_c to the leading order in ϵ is given by

$$\frac{S}{N_{T_c}} = \frac{2}{3} \frac{T_c}{\epsilon_F} = \frac{2}{3} \frac{e^{-1}}{e^{-1}} = 0.667 : \quad (89)$$

Using the Borel-Pade approximations in order to connect the two expansions above, the thermodynamic functions at $d = 3$ are found to be $P/(n_F n_{T_c})|_{T_c} = 0.172 \pm 0.022$, $E/(n_F n_{T_c})|_{T_c} = 0.270 \pm 0.004$, $\mu/\epsilon_F|_{T_c} = 0.294 \pm 0.013$, and $S/N_{T_c}|_{T_c} = 0.642$. The errors here indicate only the uncertainty due to the choice of different Pade approximations. In the recent Monte Carlo simulation,

the thermodynamic functions at the critical temperature is $P = (\mu_F N)_{j_c} = 0.207(7)$, $E = (\mu_F N)_{j_c} = 0.31(1)$, $\mu_F j_c = 0.493(14)$, and $S = N j_c = 0.16(2)$ [35]. We see that the interpolations of the two expansions indeed improve the series summations compared to the naive extrapolations from $d = 4$ or $d = 2$, while there still exist deviations between our results and the Monte Carlo simulation. We can understand these deviations partially due to the difference in the determined critical temperatures. The large deviations existing in μ_F and $S = N j_c$ may be because we know only the leading term for μ_F and the next-to-leading-order correction to S is sizable.

V. SUMMARY AND CONCLUDING REMARKS

In this paper, the thermodynamics of the Fermi gas near the unitarity limit at finite temperature has been investigated using the systematic expansion over $d = 4 - d$. We discussed that the thermodynamics in the low temperature region $T < T_c$ is dominated by the bosonic phonon excitations. The analytic formulas for the thermodynamic functions at the fixed fermion density are derived in the two limiting cases; $T \ll T_c$ in Eqs. (41)–(44) and $T \gg T_c$ in Eqs. (51)–(54).

In the high temperature region $T \gg T_c$, the fermionic quasiparticles are excited as well as the bosonic quasiparticles. We showed that the similar power counting rule of μ_F that developed at zero temperature works even above T_c . The superfluid phase transition at $T = T_c$ is of the second order. The critical temperature T_c and the thermodynamic functions around T_c were calculated to the leading and next-to-leading orders in $d - 3$. We found the critical temperature is an increasing function of the binding energy μ_b near the unitarity limit:

$$\frac{T_c}{\mu_F} = 0.260 - 0.0112 \frac{\mu_b}{\mu_F} + 0.0234 \left(\frac{\mu_b}{\mu_F}\right)^2; \quad (90)$$

The next-to-leading-order correction is reasonably small compared to the leading term even at $d = 1$. In the

unitarity limit $\mu_b = 0$, the naive extrapolation of the critical temperature to the physical case of $d = 3$ gives $T_c = \mu_F = 0.249$.

We also discussed the matching of the expansion around $d = 4$ with the expansion around $d = 2$. The critical temperature at unitarity in the expansion over $d = 2$ is given by $T_c = \mu_F = 2e^{-1} = e^{-1}$, where its naive extrapolation to $d = 1$ gives $T_c = \mu_F = 0.153$. The Borel-Pade approximations connecting the two expansions yielded $T_c = \mu_F = 0.183 - 0.014 d$ at $d = 3$, which is a moderate value located between the two naive extrapolations (Fig. 7). These values are not too far from the results obtained by the recent Monte Carlo simulations where $T_c = \mu_F = 0.15(0.25)$ [33, 35, 36]. We also applied the Borel-Pade approximations to the thermodynamic functions at T_c , which yielded $P = (\mu_F N)_{j_c} = 0.172$, $E = (\mu_F N)_{j_c} = 0.270$, $\mu_F j_c = 0.294$, and $S = N j_c = 0.642$ at $d = 3$.

The Borel-Pade approximations employed here to match the two expansions around four and two spatial dimensions do not correctly reflect large-order behaviors of the two expansions, i.e., the expansions over $d = 4 - d$ and $d = d - 2$ are most probably not convergent and hence the Borel transform $B(t)$ of such series expansions will have singularities somewhere in the complex t -plane [14]. In order for the accurate determination of the critical temperature and the thermodynamic functions at $d = 3$, it will be important to appropriately take into account the knowledge on the large-order behaviors of the expansions both around four and two spatial dimensions. The calculation of higher-order corrections to our results is also interesting for this purpose. These problems should be studied in future works.

Acknowledgments

The author would like to thank D. T. Son for useful discussions. This research was supported by the Japan Society for the Promotion of Science for Young Scientists.

-
- [1] D. M. Eagles, Phys. Rev. 186, 456 (1969).
 [2] A. J. Leggett, in Modern Trends in the Theory of Condensed Matter (Springer, Berlin, 1980).
 [3] P. Nozières and S. Schmitt-Rink, J. Low Temp. Phys. 59, 195 (1985).
 [4] K. M. O'Hara et al., Science 298, 2179 (2002).
 [5] C. A. Regal, M. G. Reiner, and D. S. Jin, Phys. Rev. Lett. 92, 040403 (2004).
 [6] M. Bartenstein et al., Phys. Rev. Lett. 92, 120401 (2004).
 [7] M. W. Zwierlein et al., Phys. Rev. Lett. 92, 120403 (2004).
 [8] J. Kinast et al., Phys. Rev. Lett. 92, 150402 (2004).
 [9] T. Bourdel et al., Phys. Rev. Lett. 93, 050401 (2004).
 [10] J. Kinast et al., Science 307, 1296 (2005).
 [11] G. Bertsch, Many-Body X Challenge, in Proceedings of the Tenth International Conference on Recent Progress in Many-Body Theories, edited by R. F. Bishop et al. (World Scientific, Singapore, 2000).
 [12] See, e.g., Q. Chen, J. Stažic, S. Tan, and K. Levin, Phys. Rep. 412, 1 (2005), and references therein.
 [13] Y. Nishida and D. T. Son, Phys. Rev. Lett. 97, 050403 (2006).
 [14] Y. Nishida and D. T. Son, Phys. Rev. A 75, 063617 (2007).
 [15] Z. Nussinov and S. Nussinov, arXiv:cond-mat/0410597.
 [16] G. Rupak, arXiv:nucl-th/0605074.
 [17] G. Rupak, T. Schaefer, and A. K. Rytjevski, arXiv:cond-mat/0607834.

- [18] C. A. R. Sa de Melo, M. Randeria, and J. R. Engelbrecht, Phys. Rev. Lett. 71, 3202 (1993).
J. R. Engelbrecht, M. Randeria, and C. A. R. Sa de Melo, Phys. Rev. B 55, 15153 (1997).
- [19] R. Haussmann, Z. Phys. B 91, 291 (1993); Phys. Rev. B 49, 12975 (1994).
- [20] M. Holland, S. J. J. M. F. Kokkeins, M. L. Chiofalo, and R. W. alser, Phys. Rev. Lett. 87, 120406 (2001).
- [21] E. Timmermans, K. Funayab, P. W. M. Ibonnia, and A. K. Kemanc, Phys. Lett. A 285, 228 (2001).
- [22] Y. Ohashi and A. Grin, Phys. Rev. Lett. 89, 130402 (2002); Phys. Rev. A 67, 033603 (2003).
- [23] J. N. M. ilstein, S. J. J. M. F. Kokkeins, and M. J. Hol-land, Phys. Rev. A 66, 043604 (2002).
- [24] A. Perali, P. Pieri, L. Pisani, and G. C. Strinati, Phys. Rev. Lett. 92, 220404 (2004).
- [25] X.-J. Liu and H. Hu, Phys. Rev. A 72, 063613 (2005).
- [26] Y. Nishida and H. Abuki, Phys. Rev. D 72, 096004 (2005).
- [27] H. Abuki, arXiv:hep-ph/0605081.
- [28] R. Haussmann, W. Rantner, S. Cerrito, and W. Zwerger, arXiv:cond-mat/0608282.
- [29] T.-L. Ho and E. J. Mueller, Phys. Rev. Lett. 92, 160404 (2004).
- [30] C. J. Horowitz and A. Schwenk, Phys. Lett. B 638, 153 (2006).
- [31] G. Rupak, arXiv:nucl-th/0604053.
- [32] M. W. ingate, arXiv:cond-mat/0502372.
- [33] A. Bulgac, J. E. D. Nut, and P. M. agierski, Phys. Rev. Lett. 96, 090404 (2006).
- [34] D. Lee and T. Schafer, Phys. Rev. C 73, 015201 (2006); Phys. Rev. C 73, 015202 (2006).
- [35] E. Burovski, N. Prokofev, B. Svistunov, and M. Troyer, Phys. Rev. Lett. 96, 160402 (2006); New J. Phys. 8, 153 (2006).
- [36] V. K. Akkineni, D. M. Ceperley, and N. Trivedi, arXiv:cond-mat/0608154.